Cutts, J., and Dyck, B., 2022, Incipient collision of the Rae and Slave cratons at ca. 1.95 Ga: GSA Bulletin, https://doi.org/10.1130/B36393.1.

Supplemental Material

Supplementary information for this manuscript comprises additional text including:

• **Text S1.** Garnet trace-element analysis methods

• **Text S2.** Garnet Lu-Hf geochronology methods, including an in-depth discussion of Lu-Hf isotope systematics

Supplementary figures include:

• **Figure S1.** Garnet major-element X-Ray maps

• **Figure S2.** Phase assemblage diagrams

• **Figure S3–S4.** Garnet trace-element maps and transects

• **Figure S5.** Monazite SEM images

• **Figure S6.** Monazite reference material results

• **Figure S7.** Monazite Concordia and weighted mean plots and normalized REE plots for unknowns

• **Figure S8.** Zircon SEM images

• **Figure S9.** Zircon reference material results

• **Figure S10.** Zircon Concordia and weighted mean plots for unknowns

• **Figure S11.** Monazite-Garnet partitioning

Supplementary tables include:

• **Table S1.** Bulk compositions used for phase equilibria modelling

• **Table S2–3.** Garnet trace-element data

• **Table S4.** Garnet Lu-Hf isotopic data

• **Table S5.** Monazite U-Pb and trace-element data

• **Table S6.** Zircon U-Pb and trace-element data

GSA Bulletin

Supporting Information for

Incipient collision of the Rae and Slave cratons at ca. 1.95 Ga

Jamie Cutts & Brendan Dyck

Department of Earth, Environmental and Geographical Sciences, University of British Columbia, Kelowna, BC, Canada

Contents of this file

Text S1 to S2
Figures S1 to S6

All data used in this manuscript available in Supplementary Tables S1-S7 at Zenodo: https://doi.org/10.5281/zenodo.6048019.

Introduction

Supplementary information for this manuscript comprises additional text including:

- Text S1: Garnet trace-element analysis methods
- Text S2: Garnet Lu-Hf geochronology methods, including an in-depth discussion of Lu-Hf isotope systematics

Supplementary figures include:

- Figure S1: Garnet major-element X-Ray maps
- Figure S2: Phase assemblage diagrams
- Figure S3-S4: Garnet trace-element maps and transects
- Figure S5: Monazite SEM images
- Figure S6: Monazite reference material results
- Figure S7: Monazite Concordia and weighted mean plots and normalized REE plots for unknowns
- Figure S8: Zircon SEM images
- Figure S9: Zircon reference material results
- Figure S10: Zircon Concordia and weighted mean plots for unknowns
- Figure S11: Monazite-Garnet partitioning

Supplementary tables include:

- Table S1: Bulk compositions used for phase equilibria modelling
- Table S2-3: Garnet trace-element data
- Table S4: Garnet Lu-Hf isotopic data
- Table S5: Monazite U-Pb and trace-element data
- Table S6: Zircon U-Pb and trace-element data

- Table S7: Laser ablation-inductively coupled plasma-mass spectrometry instrument settings and metadata
- Table S8: Student's T-test results

Text S1. Trace-element garnet transect and map

Trace element analyses of garnet were analyzed *in-situ* in thin-section at the Fipke Laboratory for Trace Element Research (FiLTER), Department of Earth, Environment and Geographic Sciences, University of British Columbia-Okanagan. Analyses were done using a Photon Machines Analyte ArF excimer (λ = 193 nm) laser ablation (LA) system coupled to an Agilent 8900 triple quadrapole inductively coupled plasma-mass spectrometer (ICP-MS) operated in single quad mode. All trace-element garnet data are provided in Supplementary Tables S2-S3 and trace-element profiles and maps are shown in Supplementary Figures S3-S4.

Text S2. Garnet Lu-Hf geochronology

S2.1 Methods:

All sample preparation, chemical procedures, and analyses were done at the Pacific Centre for Isotopic and Geochemical Analysis, Department of Earth, Ocean and Atmospheric Sciences, University of British Columbia-Vancouver. Garnet was extracted by wrapping the samples in parafilm prior to being gently crushed between two steel plates and using a hammer to apply pressure. Grains or fragments were then handpicked from crushed material. Whole-rock powders were prepared using an agate mortar and pestle. Both garnet and whole-rock aliquots were weighed into screw-top PFA beakers. Garnet aliquots were rinsed twice with de-ionized water and bathed in 1N HCl at room temperature for 1 hr. Prior to dissolution, both garnet and WR aliquots were admixed with a ^{176}Lu-^{180}Hf isotope tracer that approximately matched the respective Lu/Hf. Garnet dissolution was done by successive addition of a 4:2:1 mixture of concentrated HF-HNO_3-$HClO_4$ interspersed with HCl and left on a hot-plate at 120 °C for up to 15 hours for each step; solutions were dried down between each acid addition step (Lagos et al. 2007). Whole-rock powders were dissolved using two methods: 1) using 4:2 HF-HNO_3 in autoclave digestion vessels kept at high pressure (HP) and a temperature of 180 °C for 5 days and 2) using the same table-top (TT) method as garnet aliquots. Isolation of Lu and Hf was done using the cation exchange column chemistry procedures of Münker et al. (2001) and these were subsequently purified by re-loading onto the columns using ascorbic acid following the methods of Sprung et al. (2010).

Lu and Hf isotope analyses were done using a Nu Instruments *NuPlasma* multi-collector inductively coupled plasma mass spectrometer. The ^{176}Lu/^{175}Lu of unknowns was determined by constraining the isobaric interference of ^{176}Yb on ^{176}Lu using a run-specific empirically calibrated linear correlation between ln(^{176}Yb/^{171}Yb)-ln(^{174}Yb/^{171}Yb) as determined by replicate Yb standard measurements on a given day (Blichert-Toft et al., 2002). Hf mass bias was corrected by assuming exponential-law behaviour (^{179}Hf/^{177}Hf = 0.7325). All Hf isotope analyses of unknowns were normalized to ATI-475 Hf, which was developed as an in-house reference material from metal ingots that are isotopically identical to the original JMC-475 metal (^{176}Hf/^{177}Hf = 0.282160; Vervoort and Blichert-toft 1999). Uncertainty on ^{176}Lu/^{177}Hf was conservatively estimated to be 0.25%, which represents the long-term external reproducibility of this ratio as estimated from whole-rock reference material analysis. The ^{176}Hf/^{177}Hf external reproducibility of unknowns was estimated based on the external repeatability of ^{176}Hf/^{177}Hf of repeated analyses of ATI-475 analysed at concentrations that bracket those of the unknowns (Bizzaro et al. 2003). Total procedural blanks during the course of our analytical sessions were 7-11 pg Hf. Isochron regressions and age calculations were done using IsoplotR (Vermeesch, 2018) and a λ^{176}Lu of $1.867 \cdot 10^{-11}$ yr-1 (Scherer et al., 2001; Söderlund et al., 2004). The Lu-Hf isotope data are provided in Supplementary Table S4.

S2.2. Discussion of the influence of inherited Hf-bearing phases on Lu-Hf isotope systematics

Co-dissolution of inherited Hf-bearing phases represents an important source of contamination and skewing of Lu-Hf isotope systematics. The most common phases of interest in this regard are zircon, rutile, and ilmenite (Baxter and Scherer, 2013), as they may contain >1 wt% Hf (Rubatto, 2017), are refractory, and resistant to thermal resetting. In the case of dissolution of a phase that is in chemical equilibrium with garnet and the whole rock (i.e., developed at a similar time), the additional Hf will only serve to draw the aliquot of interest down the isochron, resulting in a lower $^{176}Lu/^{177}Hf$, less spread on the isochron, and potentially lower precision on the date. On the other hand, in the case of dissolution of a phase with inherited Hf, which is thus, not in chemical equilibrium with garnet or the whole-rock—most common in the case of zircon—the aliquot of interest will have lower $^{176}Hf/^{177}Hf$ than the rest of the assemblage and most commonly produces excess scatter in the regression (Scherer et al. 2000; Baxter and Scherer, 2013).

This co-dissolution of Hf-bearing inclusions is exemplified in the results for sample C53. Garnet aliquots and the low-pressure whole rock are dissolved in such a way to leave behind any refractory phases, such as zircon and this has resulted in an isochron with no excess scatter (Lagos et al. 2007). In contrast, the whole rock prepared using high-pressure autoclave dissolution has a lower $^{176}Hf/^{177}Hf$ and plots below the isochron regression of the other aliquots and, if included, would result in excess scatter and a geologically meaningless date.

Counter-intuitively, the low-pressure whole rock contains significantly more Hf than the aliquot prepared using high-pressure dissolution; however, this likely reflects the heterogeneous and domainal nature of the pelitic sample C53. Evidence for this includes:

1) The chemically heterogeneous nature of the pelitic protolith has resulted in garnet and zircon mostly occurring within a single layer in the matrix.
2) The sample comprised a 2.5 cm-diameter x 2-3 cm long rock core and this was dominated by a 1 cm-diameter garnet, which was extracted for the garnet aliquots; the sample contained other smaller garnet as well.
3) The analyzed garnet fragments were Hf-rich, some (e.g., Grt-3) to a similar extent to the whole-rock.
4) Each whole-rock aliquot comprised ~50 mg of powder that was extracted from a 200-300 mg.

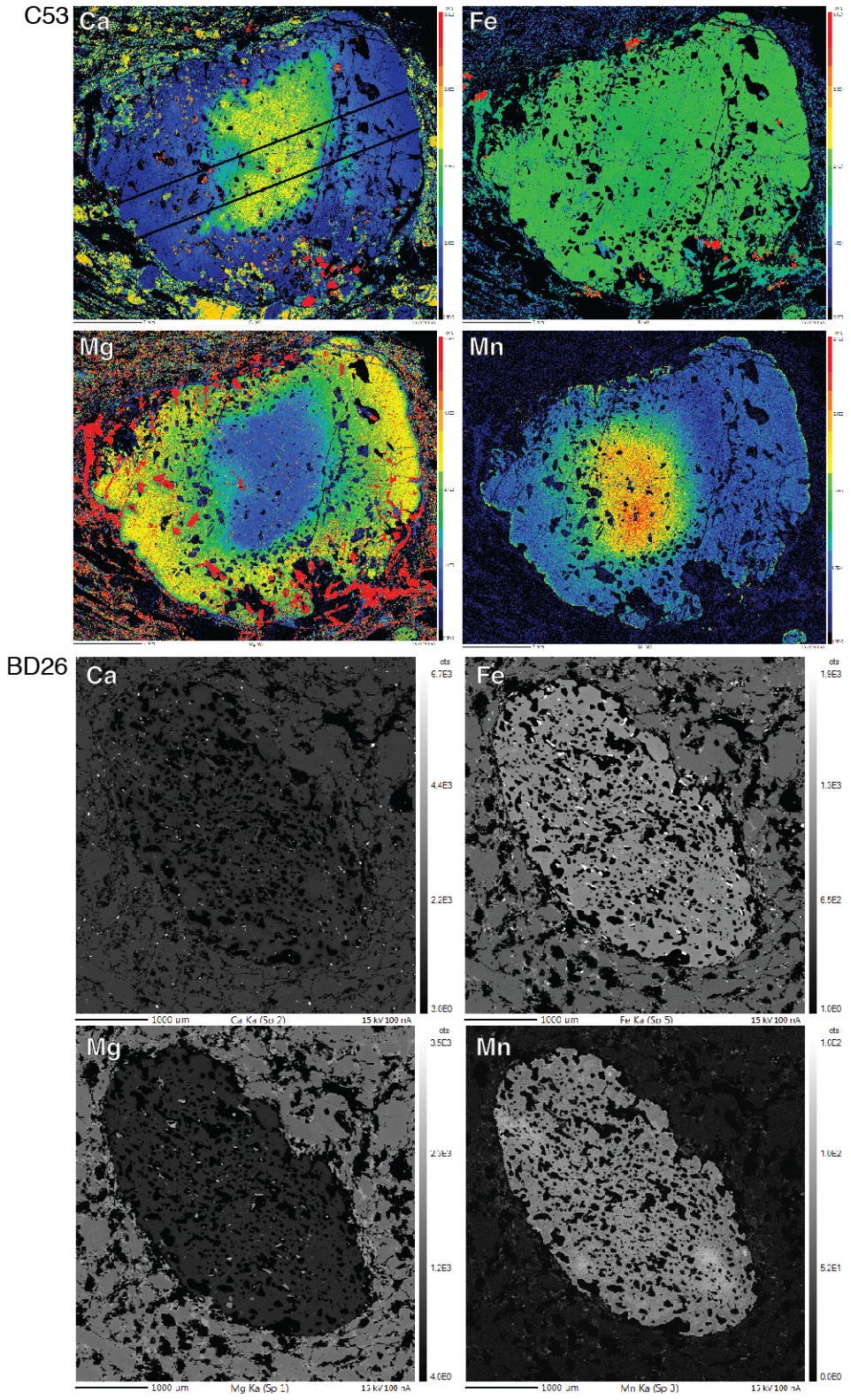

Figure S1. Garnet major-element X-Ray maps

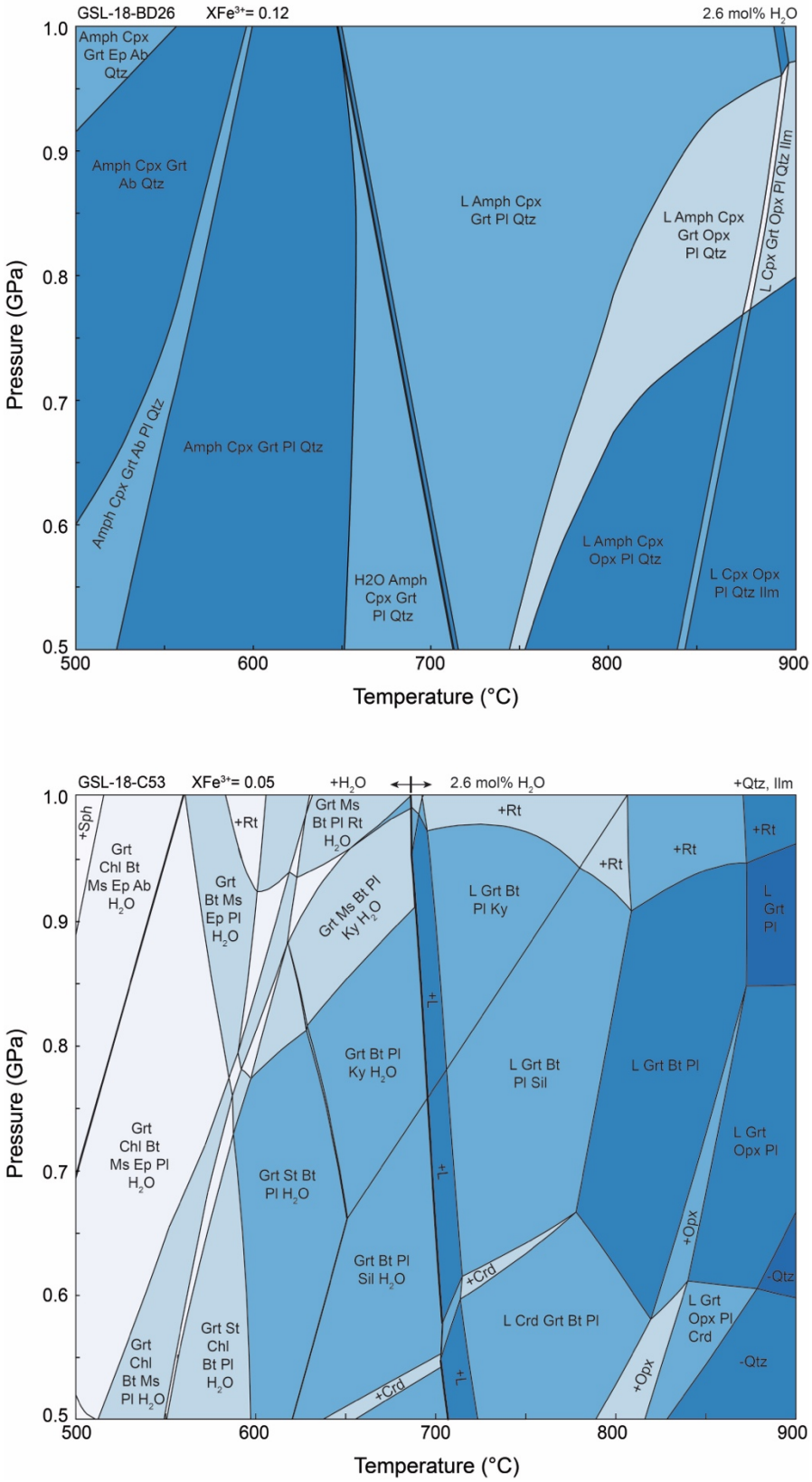

Figure S2. Phase assemblage diagrams

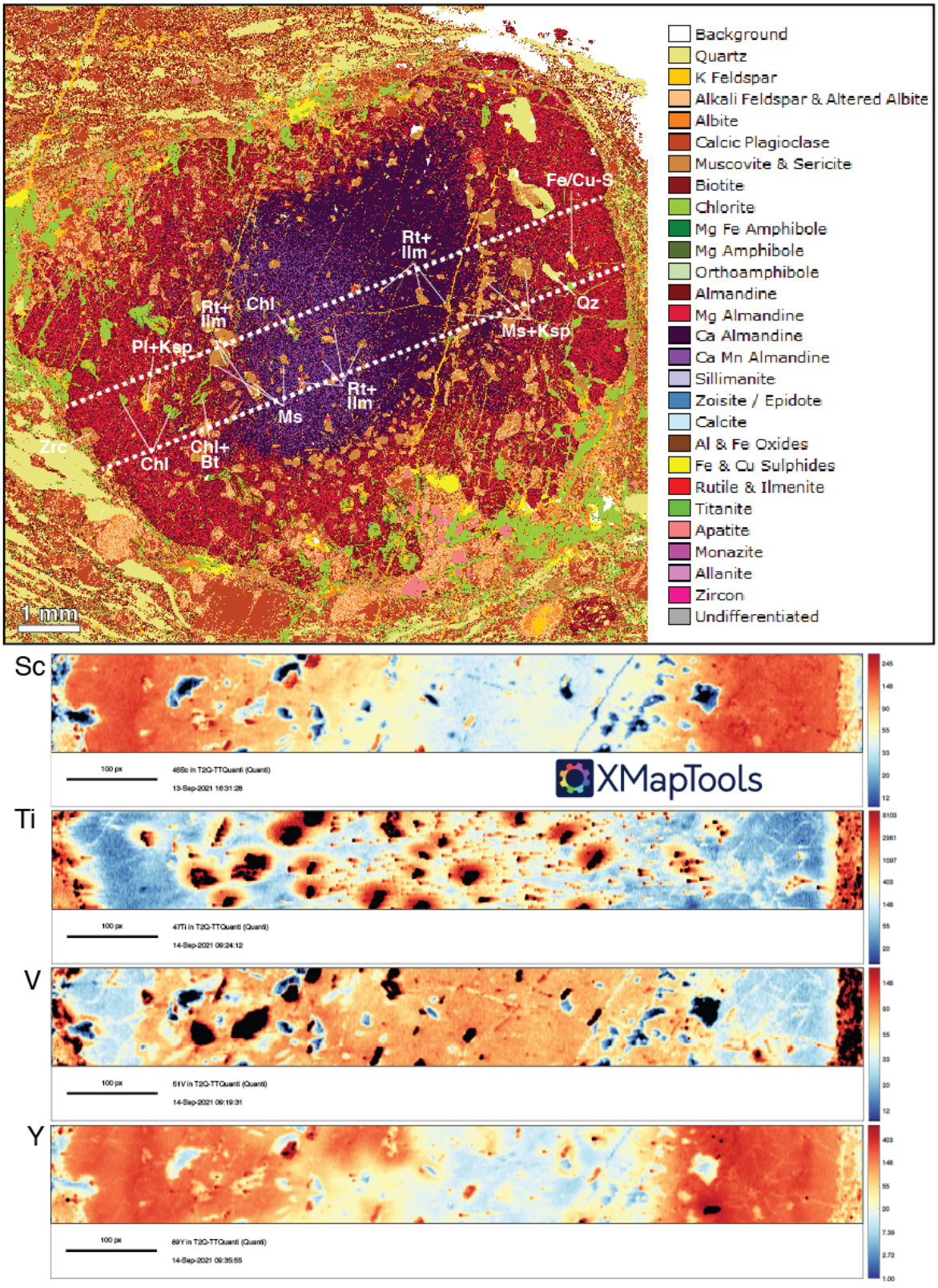

Figure S3-1. Garnet trace-element maps for sample C53

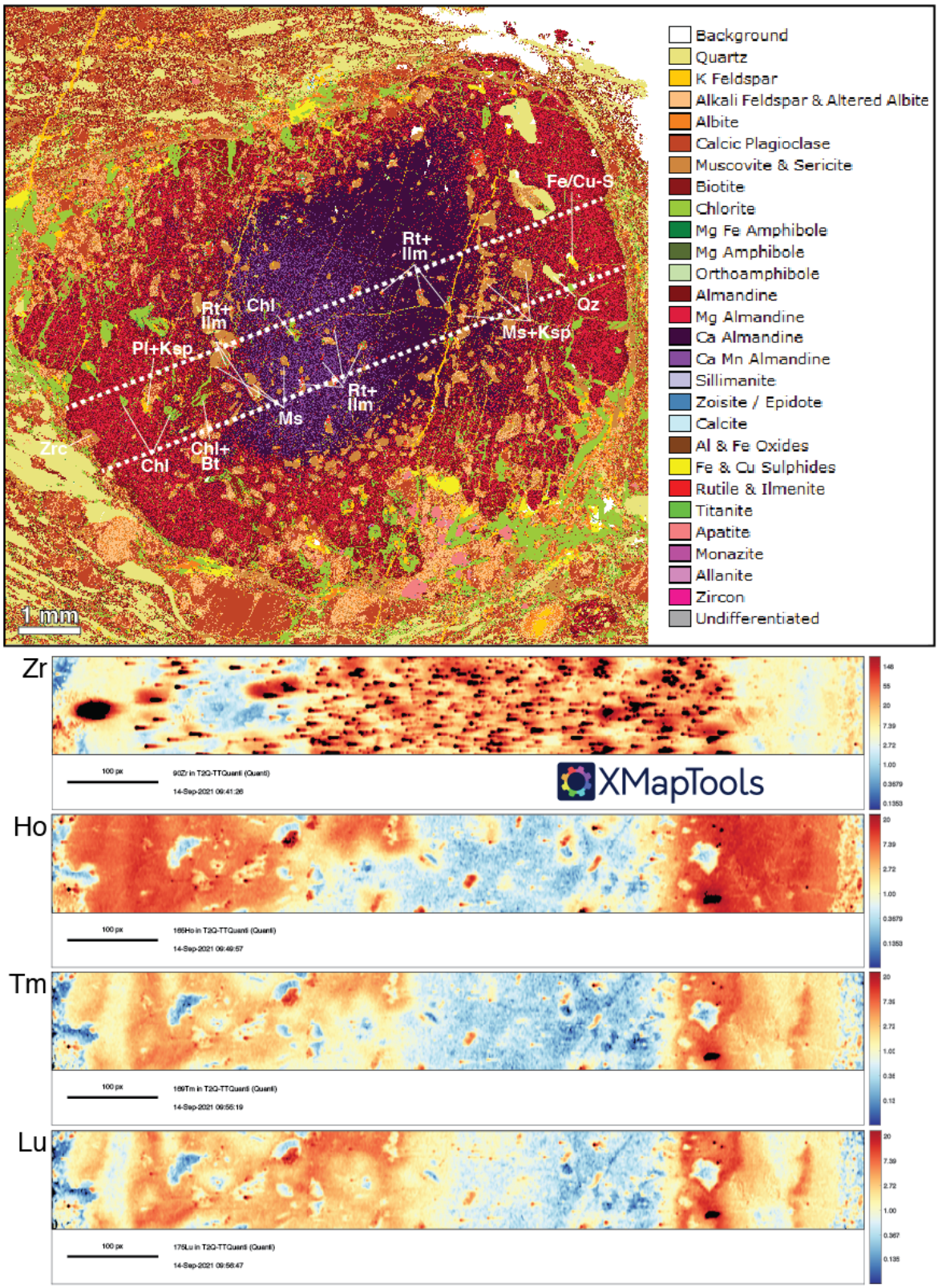

Figure S3-1 con't. Garnet trace-element maps for sample C53

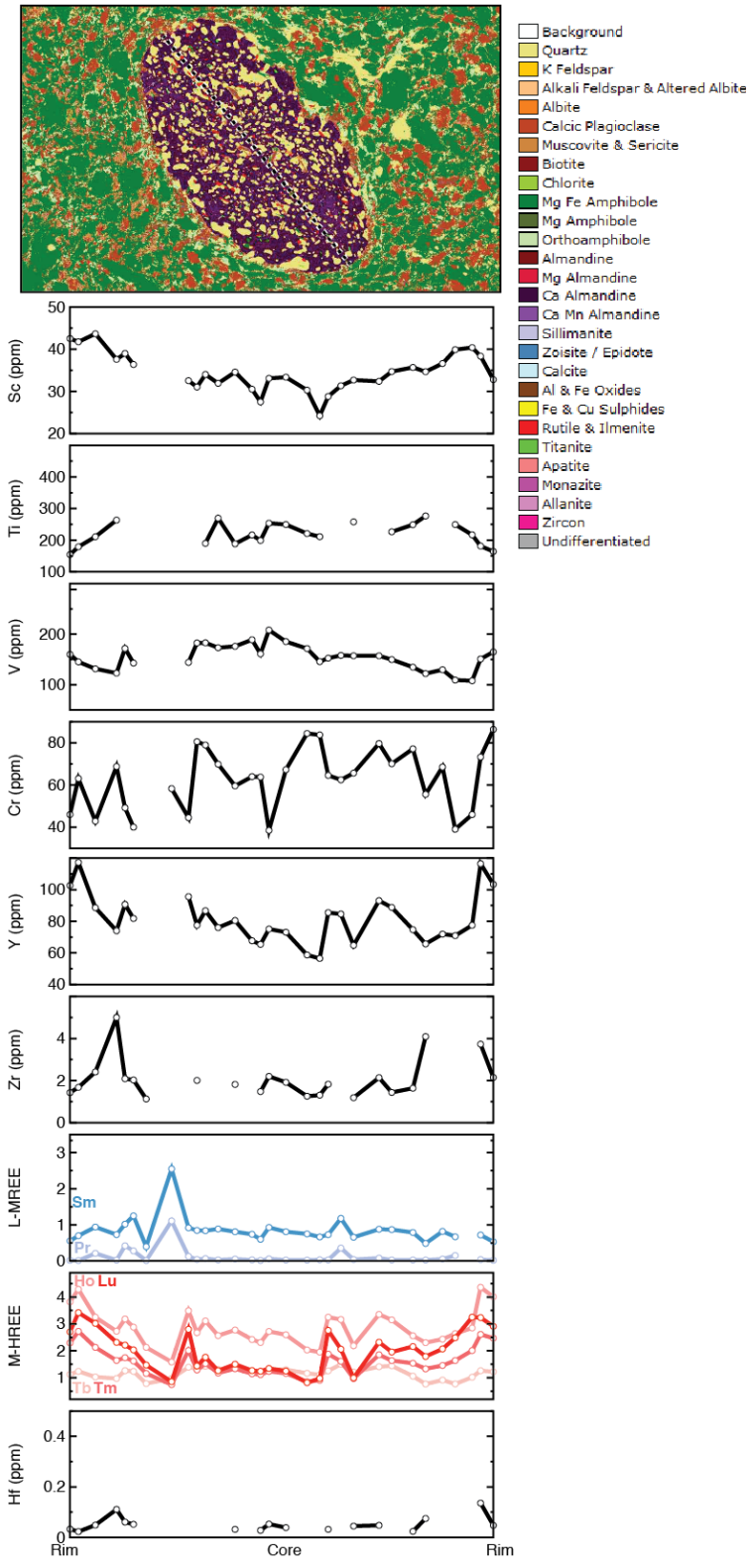

Figure S4. Garnet trace-element profiles for sample BD26

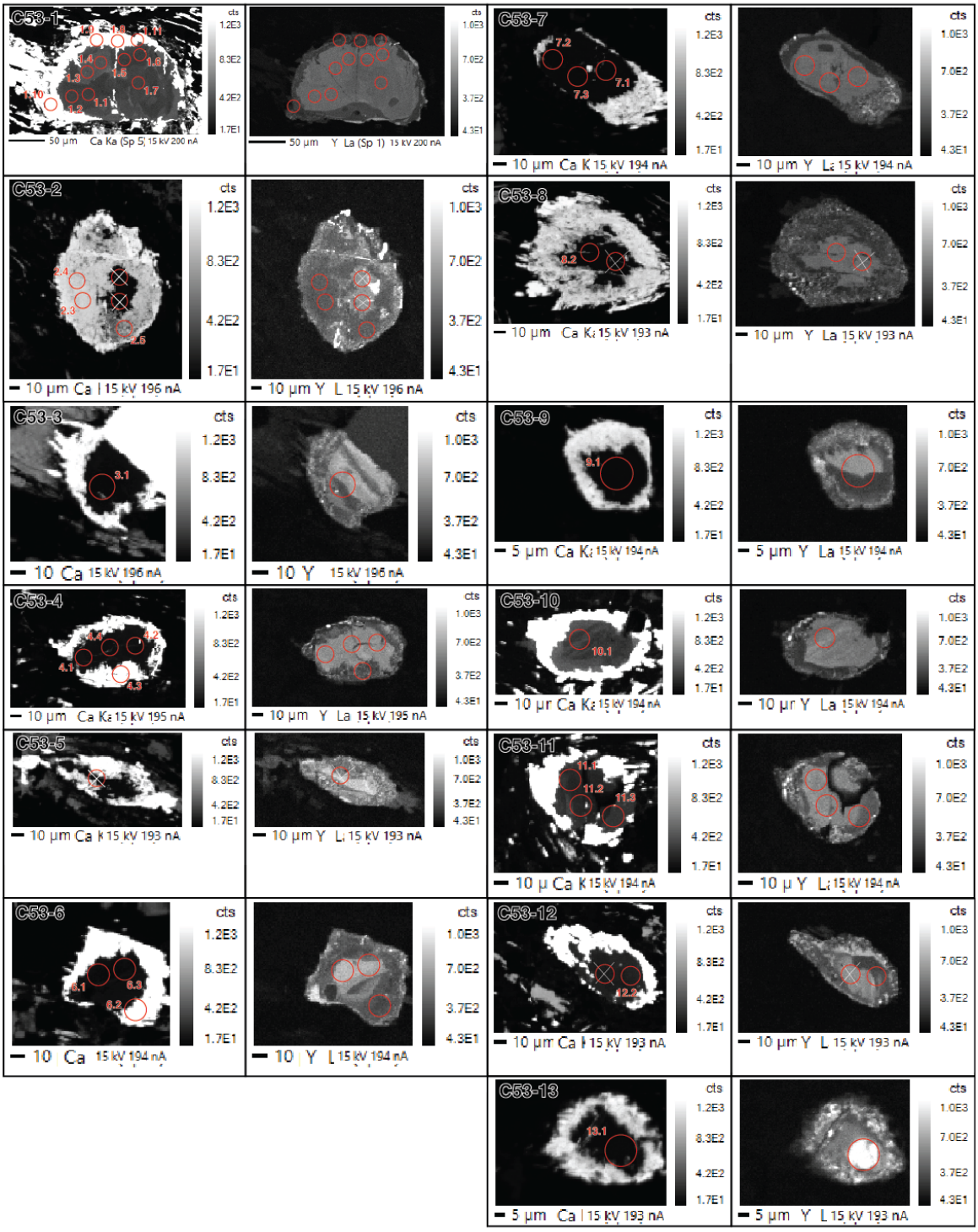

Figure S5-1. Scanning Electron Microscope Ca and Y maps of monazite

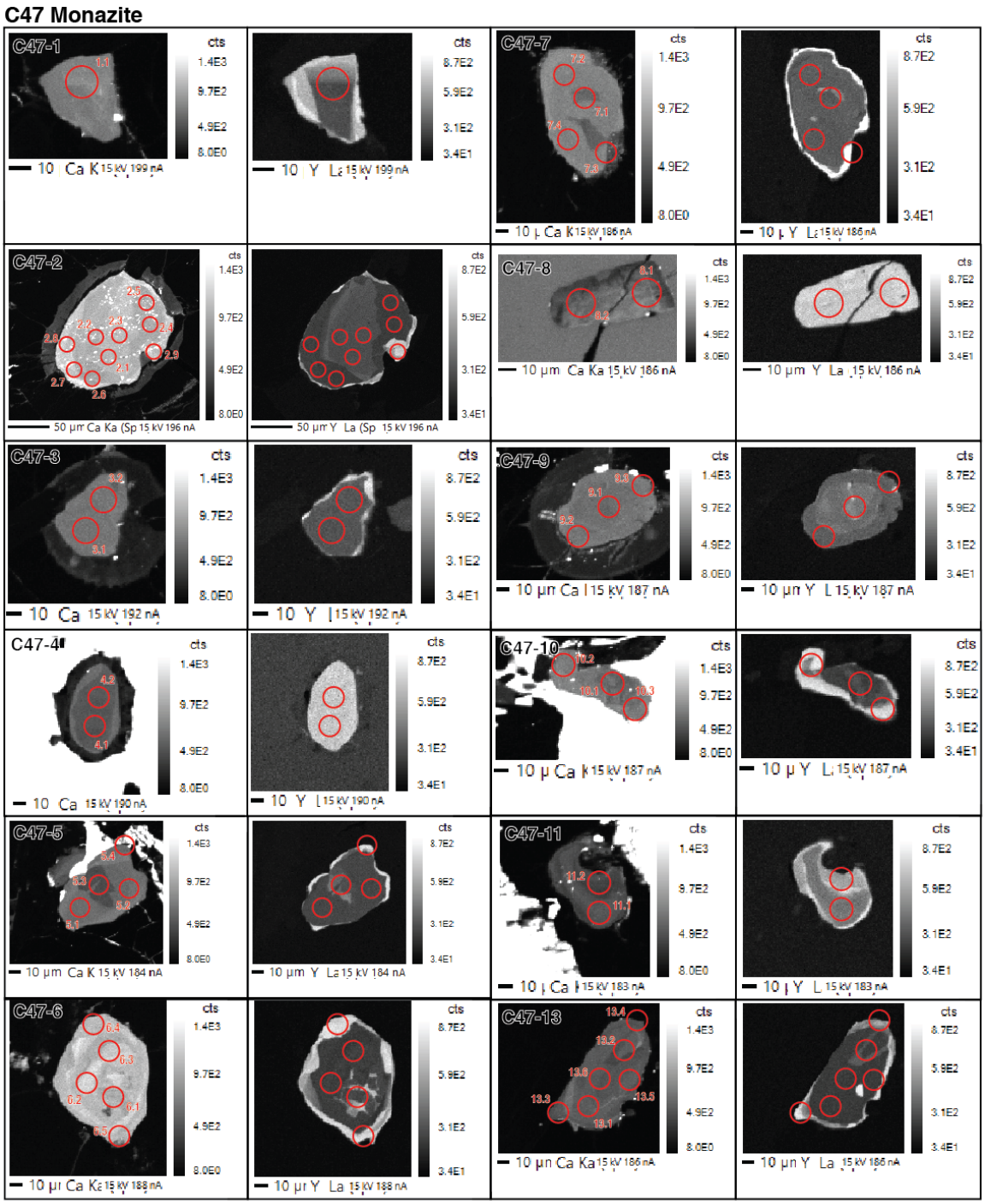

Figure S5-2. Scanning Electron Microscope Ca and Y maps of monazite

BD25 Monazite

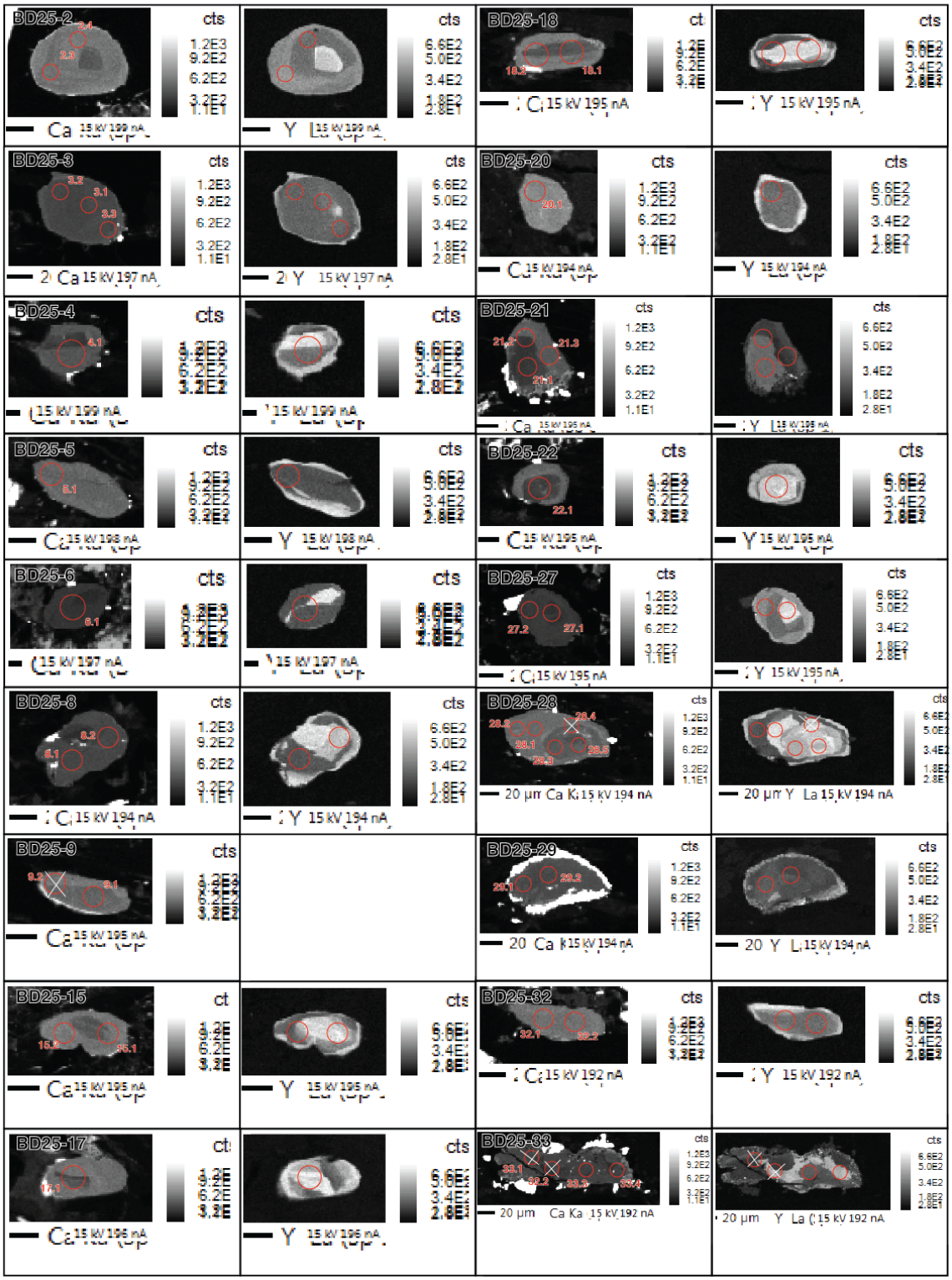

Figure S5-3. Scanning Electron Microscope Ca and Y maps of monazite

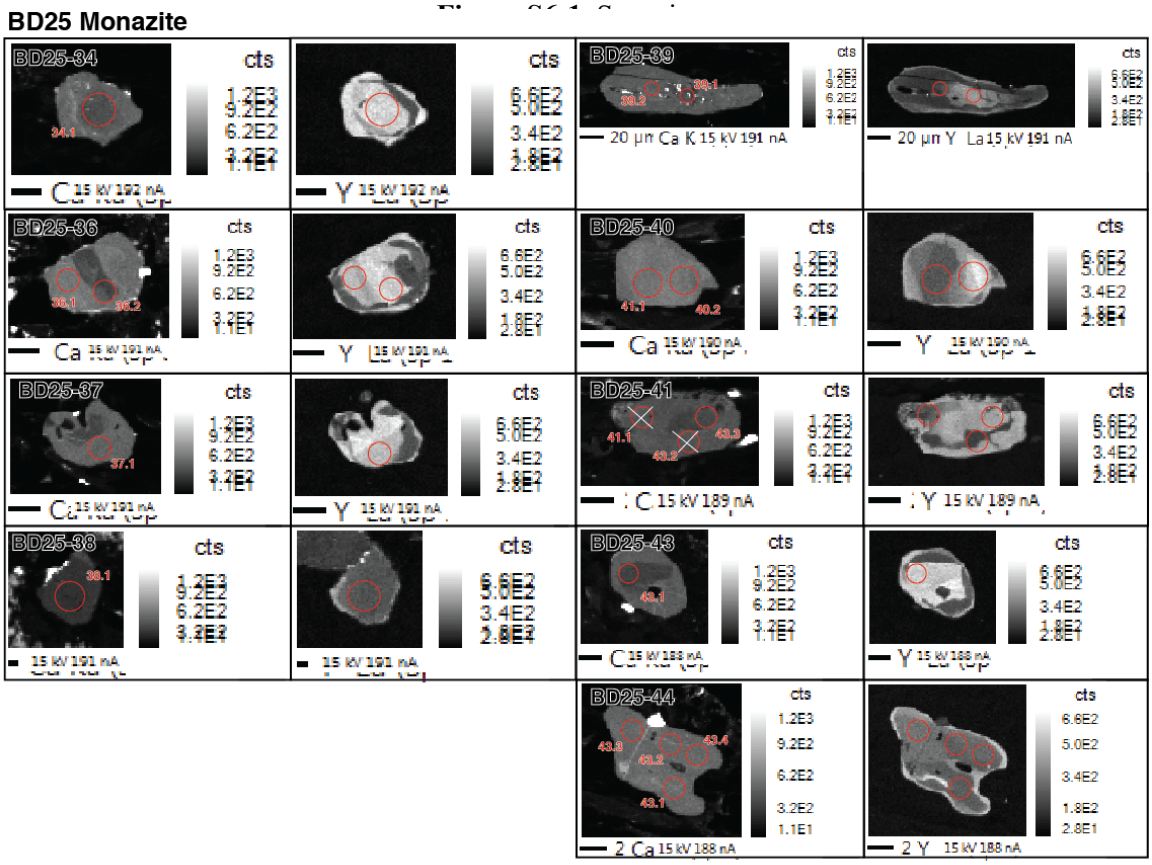

Figure S5-4. Scanning Electron Microscope Ca and Y maps of monazite

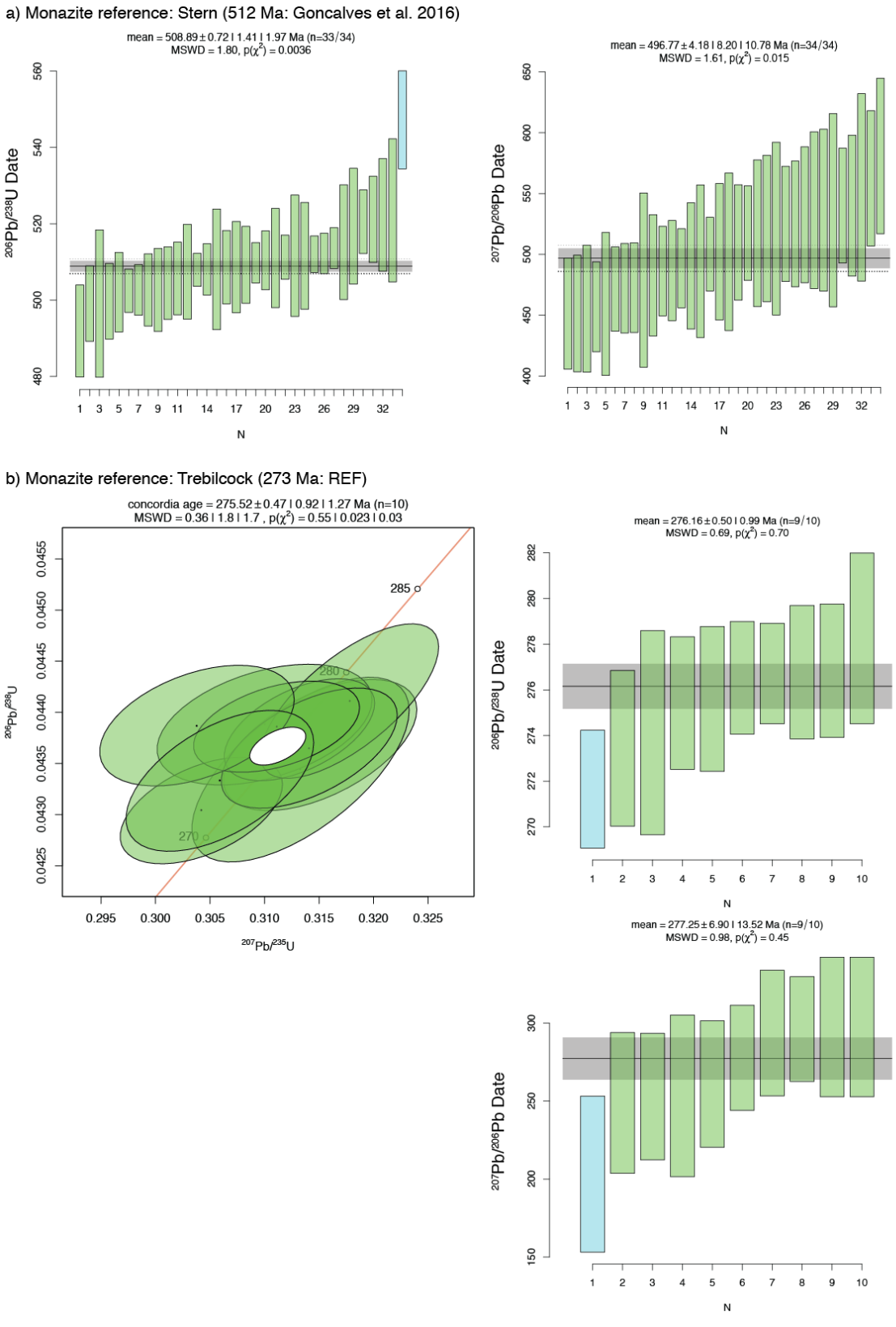

Figure S6-1. U-Pb results for reference materials

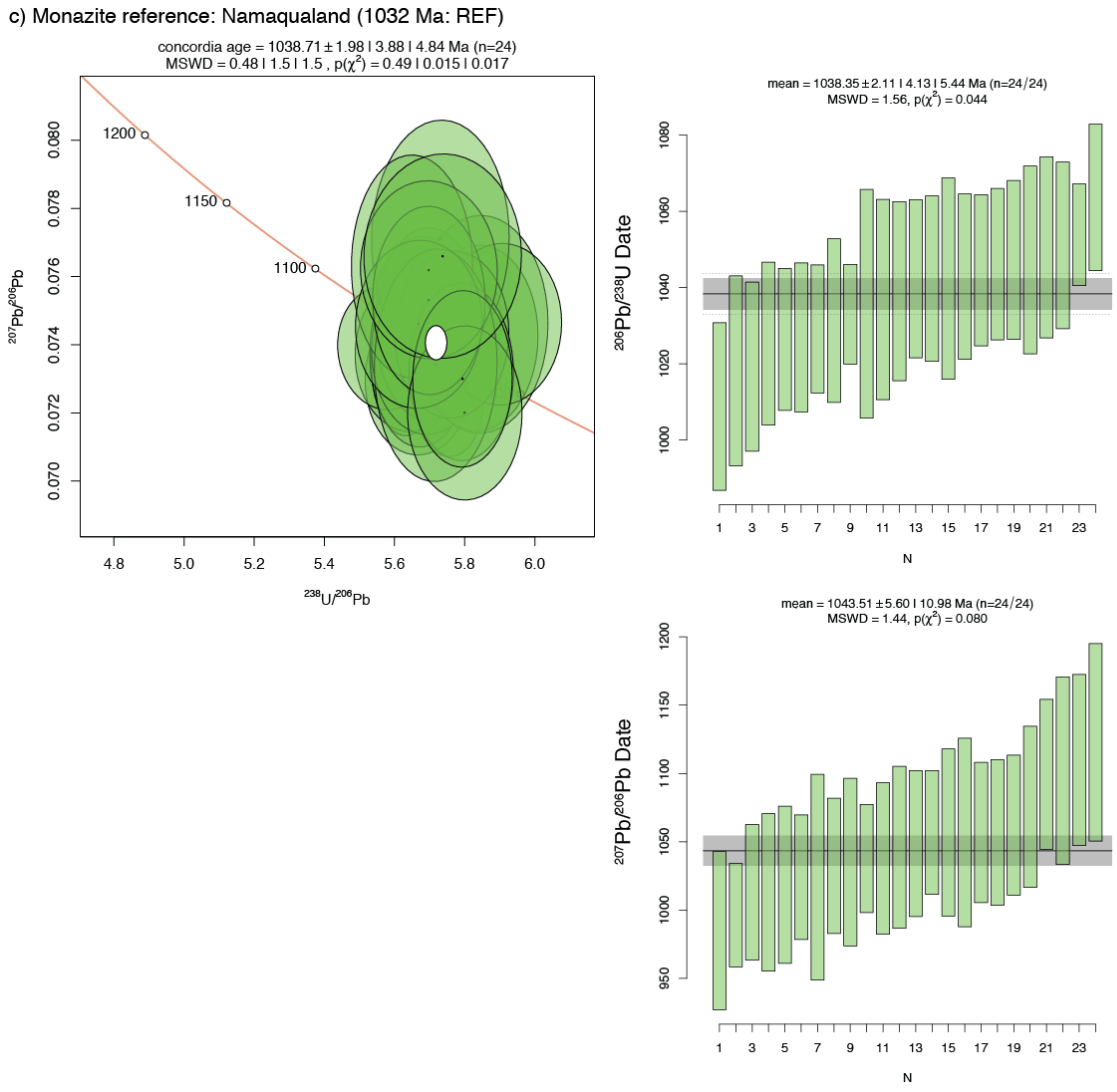

Figure S6-2. U-Pb results for reference materials

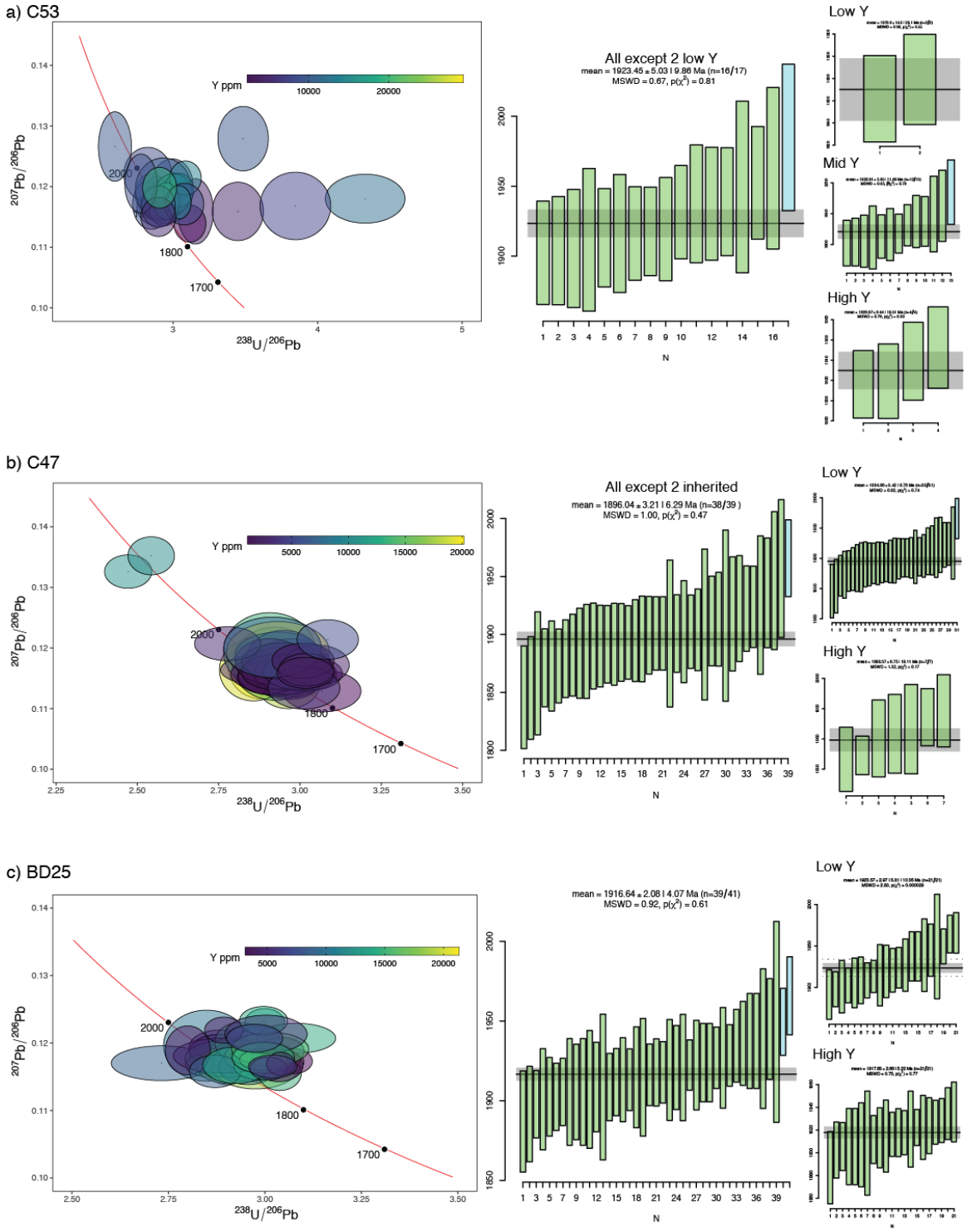

Figure S7. U-Pb results for monazite unknowns

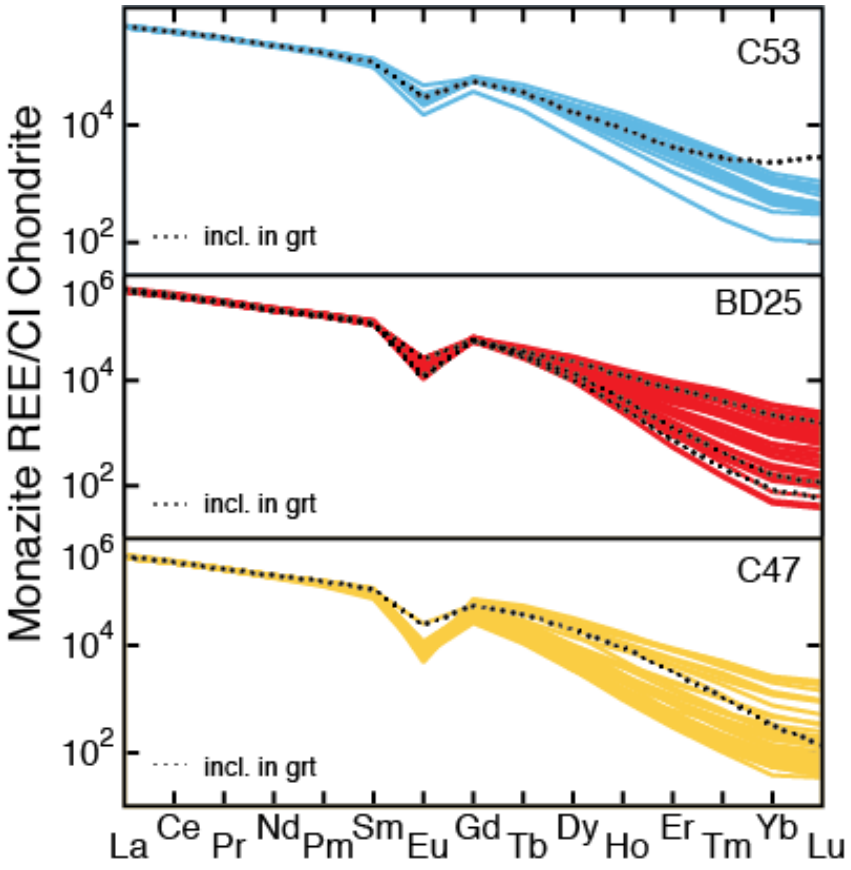

Figure S7 con't. Chondrite-normalised REE plots for monazite unknowns

C53 Zircon

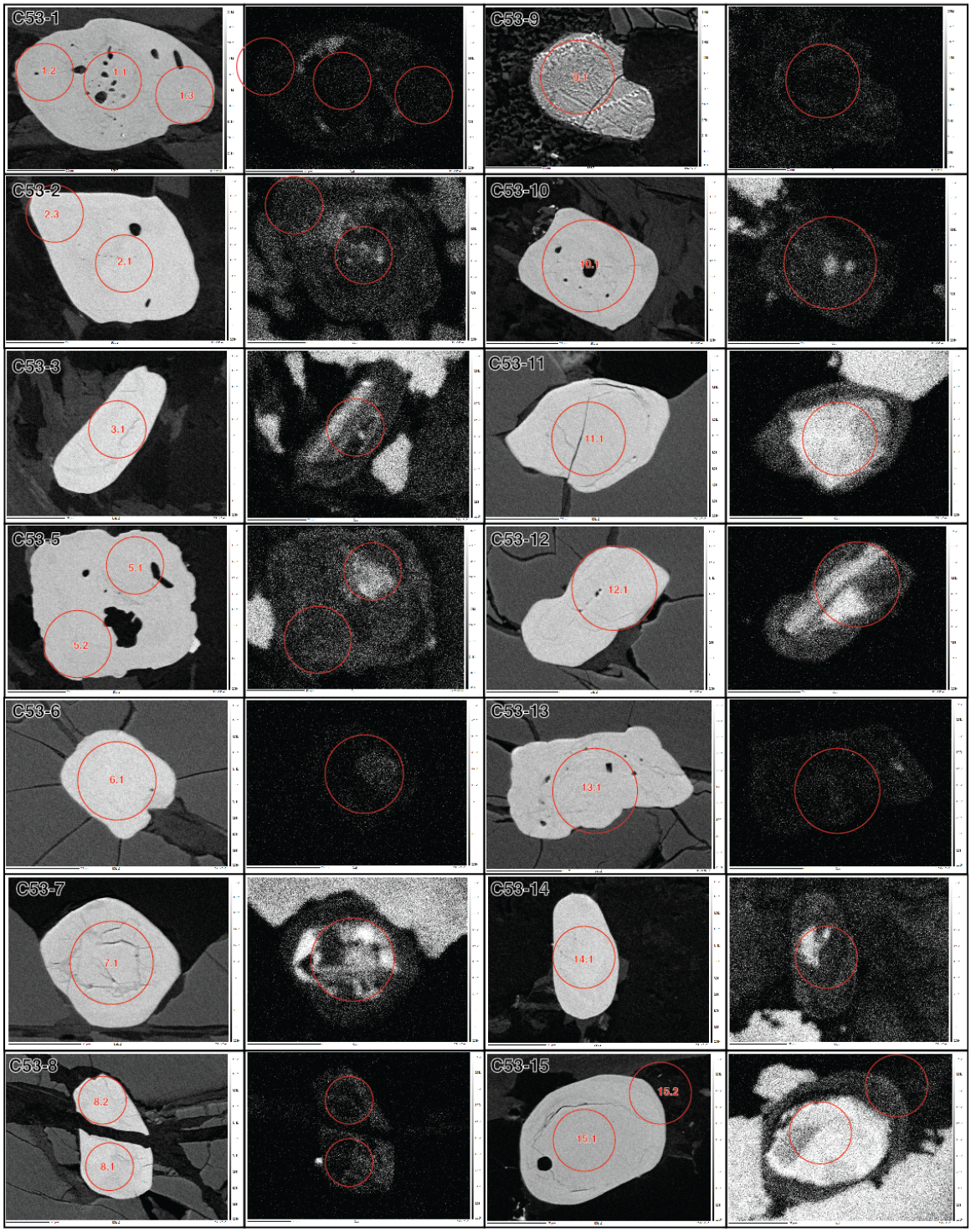

Figure S8-1. Scanning Electron Microscope back-scattered electron and cathodoluminescence images of zircon

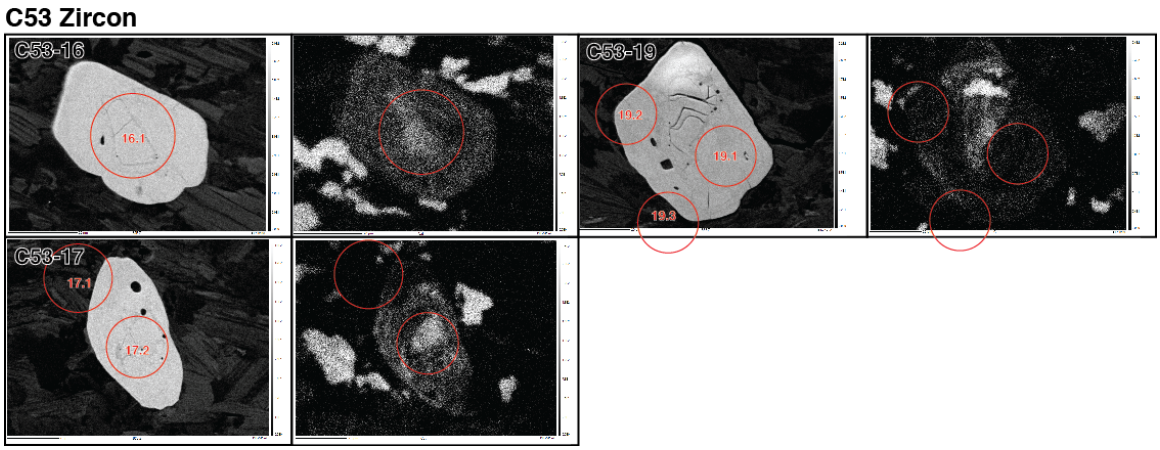

Figure S8-2. Scanning Electron Microscope back-scattered electron and cathodoluminescence images of zircon

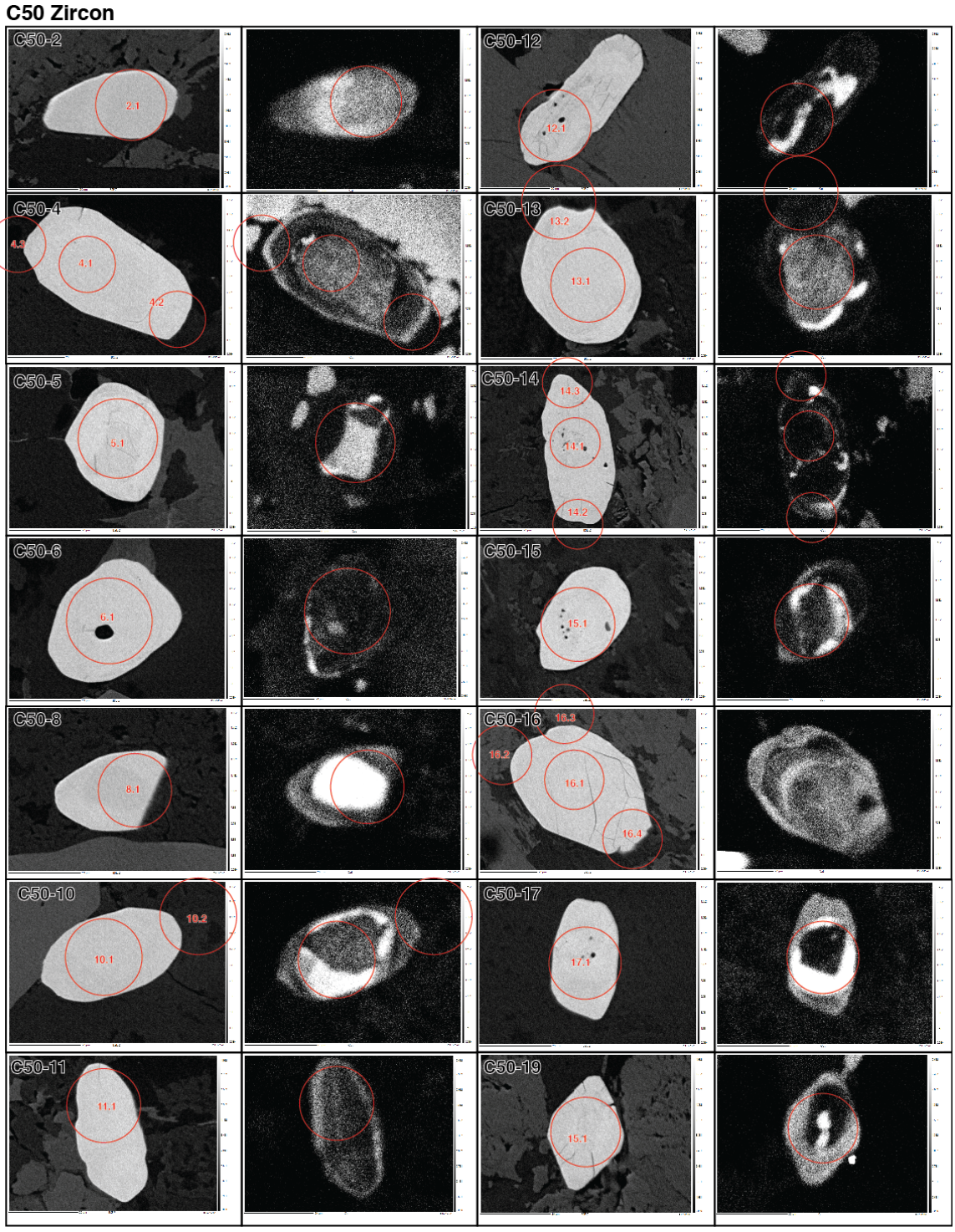

Figure S8-3. Scanning Electron Microscope back-scattered electron and cathodoluminescence images of zircon

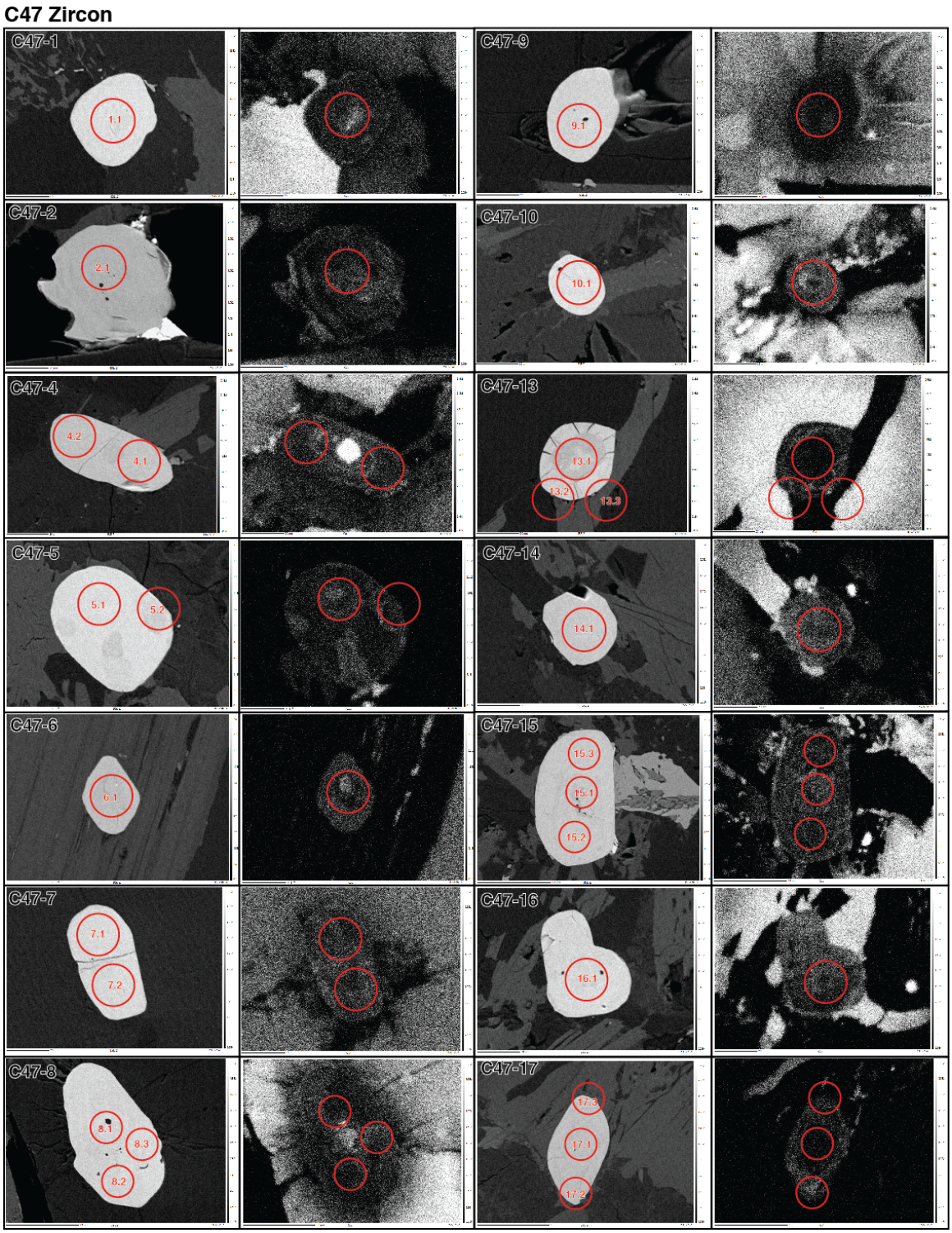

Figure S8-4. Scanning Electron Microscope back-scattered electron and cathodoluminescence images of zircon

C47 Zircon

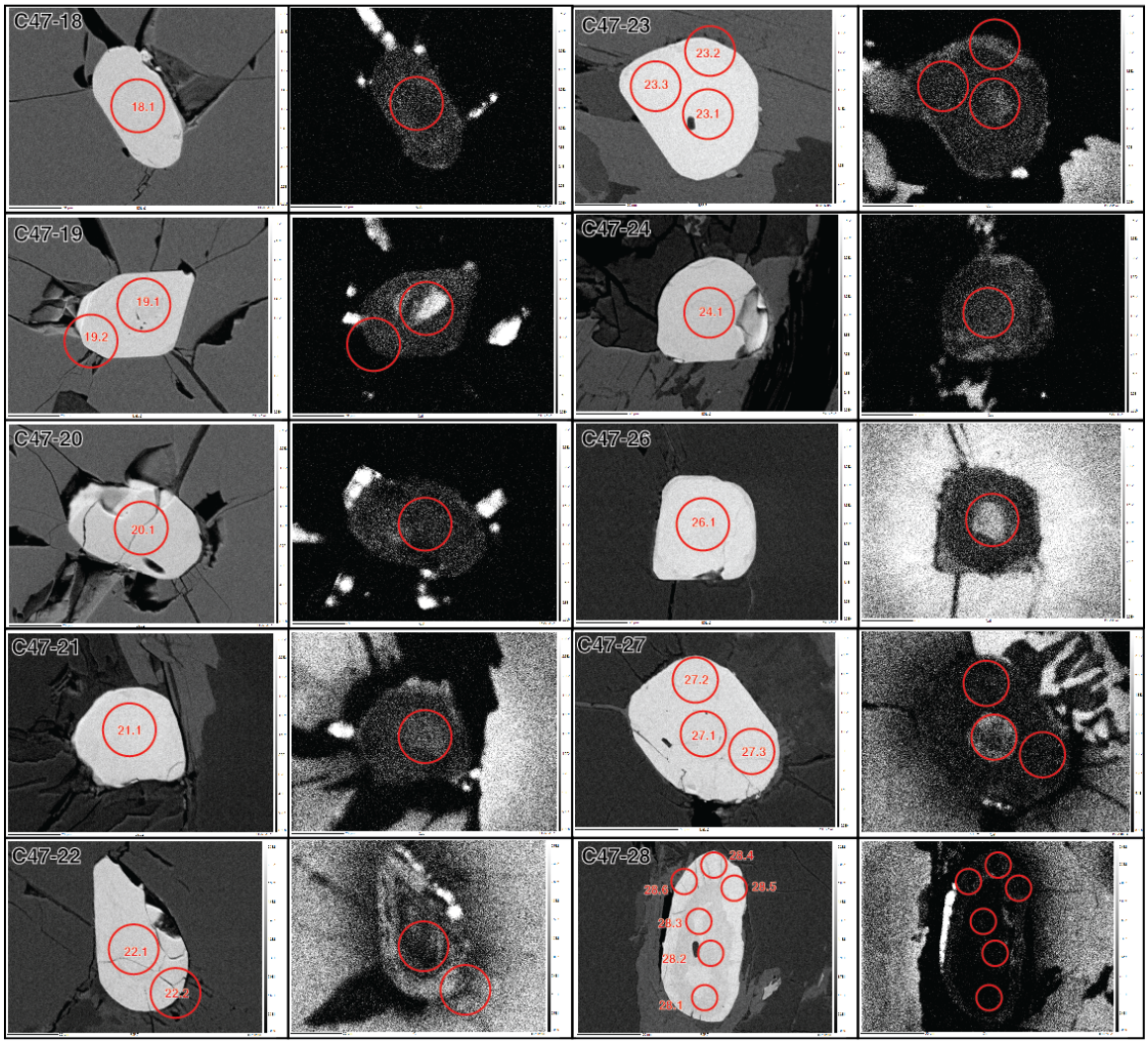

Figure S8-5. Scanning Electron Microscope back-scattered electron and cathodoluminescence images of zircon

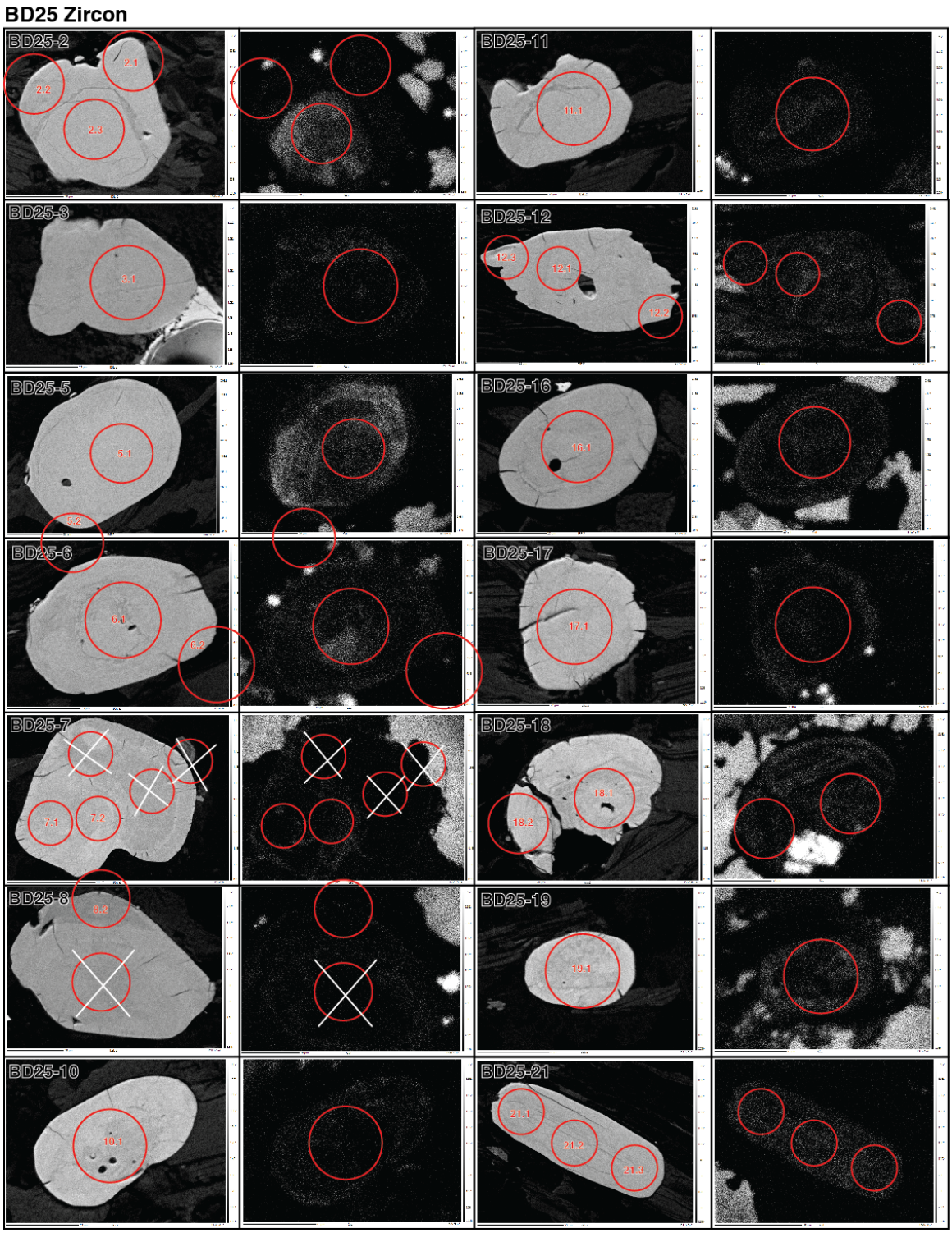

Figure S8-6. Scanning Electron Microscope back-scattered electron and cathodoluminescence images of zircon

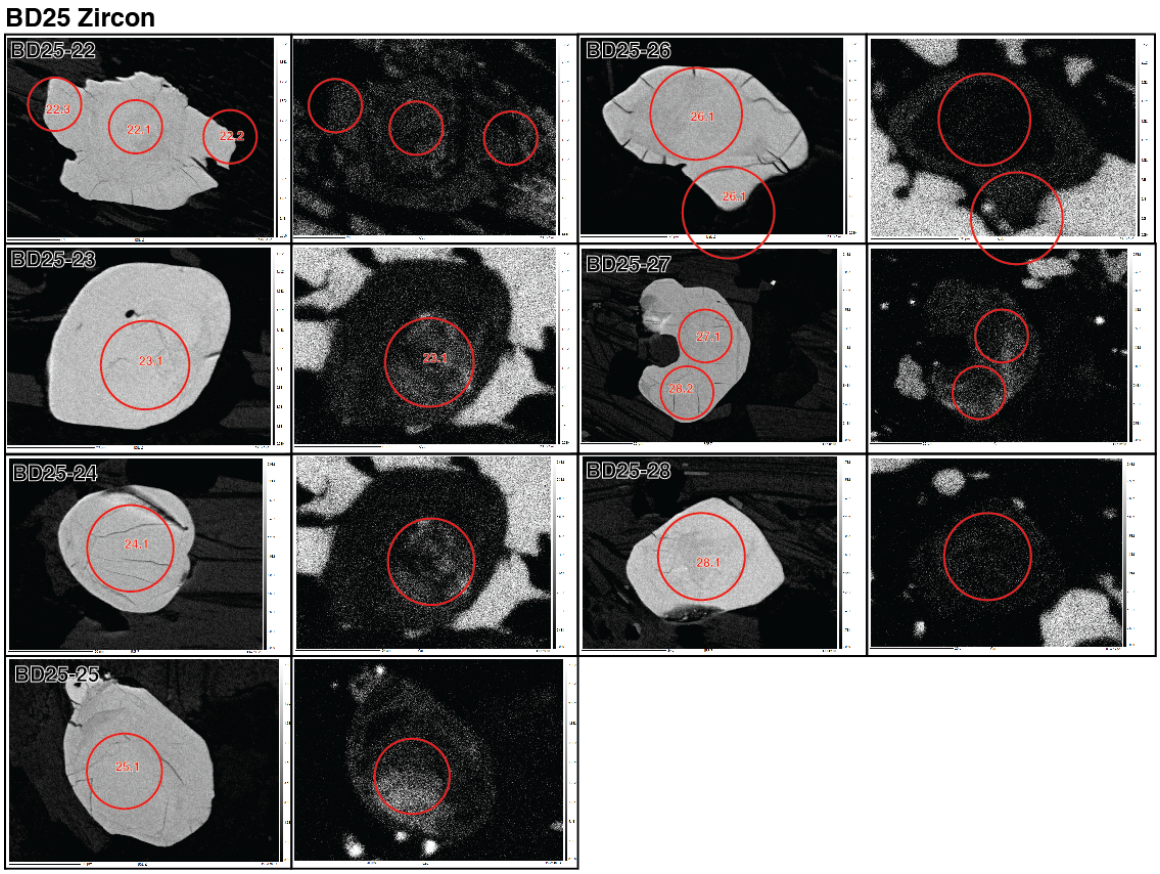

Figure S8-7. Scanning Electron Microscope back-scattered electron and cathodoluminescence images of zircon

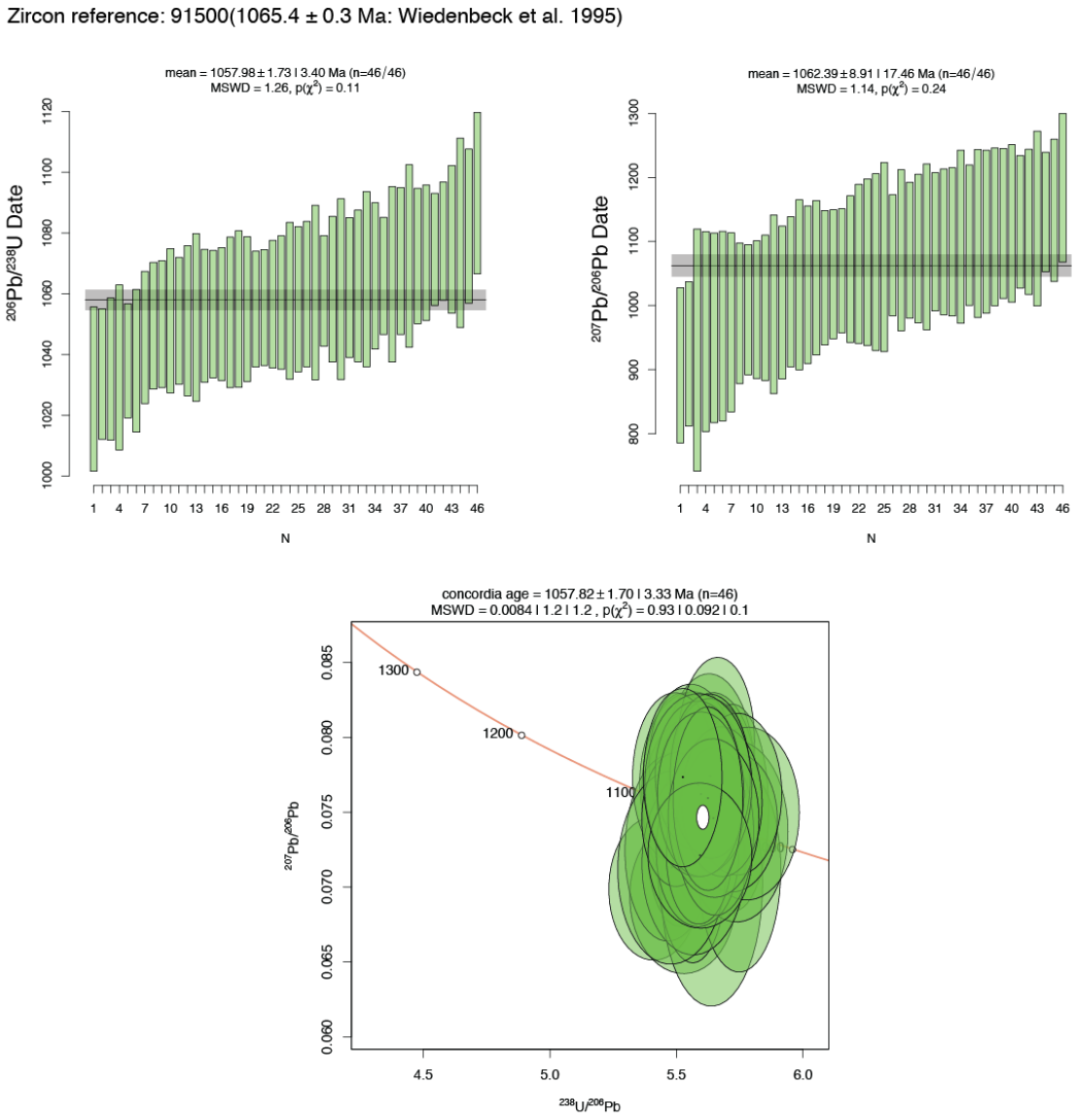

Figure S9. U-Pb results for zircon reference material 9100

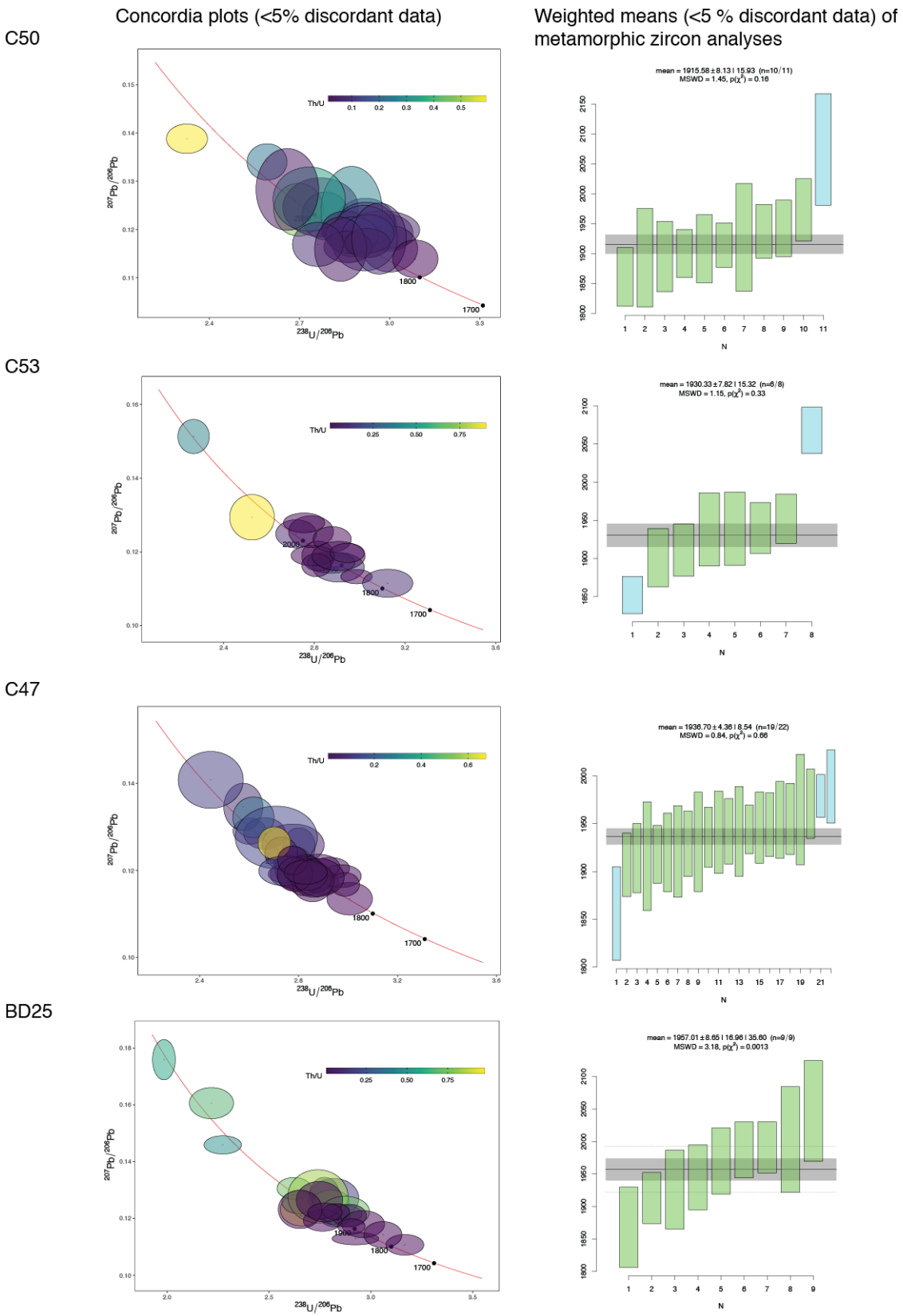

Figure S10. U-Pb results for zircon unknowns

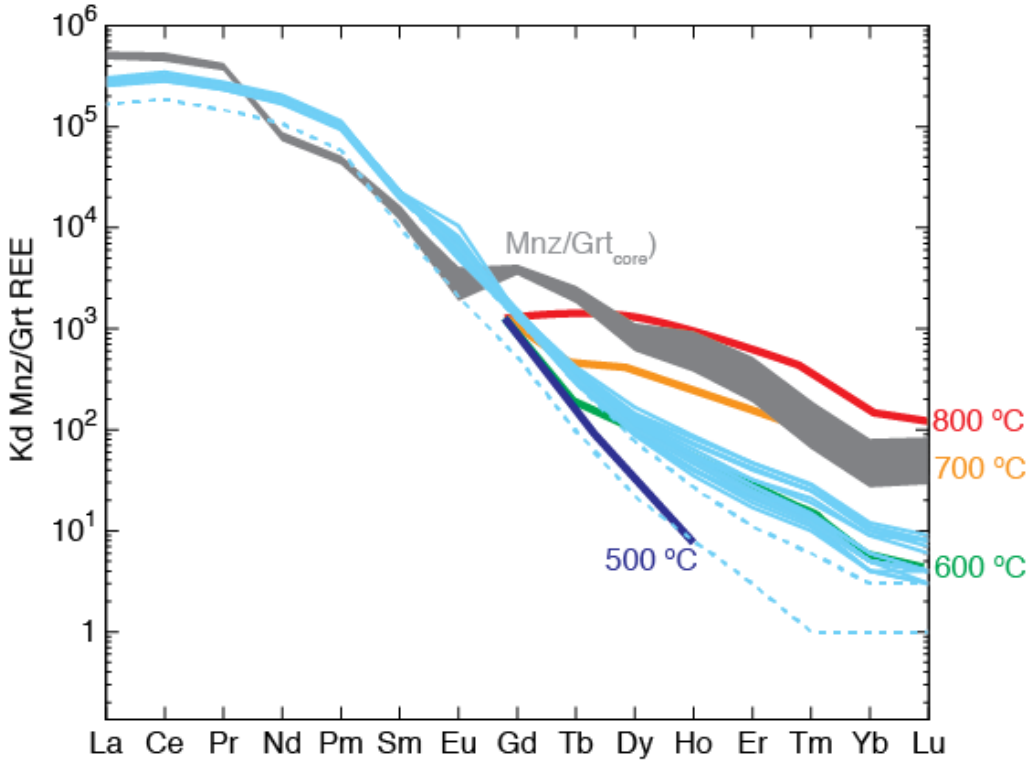

Figure S11. Monazite-garnet partitioning after Hacker et al. (2019). Several assumptions required to use such a relationship are not met with sample C53, namely that garnet and monazite were the only REE-bearing phases growing. Consequently, the results shown here are inconsistent with results from petrological modelling, which we posit are likely more accurate, namely: the monazite-garnet$_{core}$ shows equilibrium temperatures of 700-800 C and the monazite-garnet$_{rim}$ temperatures of 500-600 C. These temperatures are the reverse to what is predicted by modelling results that infer garnet core to have begun growing at 550-600 C and the rim to have grown supra-solidus at 750 C.

References

Aleinikoff, J.N., Schenck, W.S., Plank, M.O., Srogi, L.A., Fanning, C.M., Kamo, S.L., and Bosbyshell, H., 2006, Deciphering igneous and metamorphic events in high-grade rocks of the Wilmington complex, Delaware; morphology, cathodoluminescence and backscattered electron zoning, and SHRIMP U-Pb geochronology of zircon and monazite: Geological Society of America Bulletin, v. 118, p. 39-64.

Baxter, E.F., and Scherer, E.E., 2013, Garnet Geochronology: Timekeeper of Tectonometamorphic Processes: Elements, v. 9, p. 433–438.

Bizzarro, M., Baker, J.A., and Ulfbeck, D., 2003, A New Digestion and Chemical Separation Technique for Rapid and Highly Reproducible Determination of Lu/Hf and Hf Isotope Ratios in Geological Materials by MC-ICP-MS: Geostandards and Geoanalytical Research, v. 27, p. 133–145.

Blichert-Toft, J., Boyet, M., Télouk, P., and Albarède, F., 2002, Sm-Nd and Lu-Hf in eucrites and the differentiation of the HED parent body: Earth and Planetary Science Letters, v. 204, p. 167–181.

Dyck, B., Goddard, R.M., Wallis, D., Hansen, L.N., and Martel, E., 2021, Metamorphic evolution of the Great Slave Lake shear zone: Journal of Metamorphic Geology, v. 39, p. 567-590.

Goncalves, G.O., Lana, C., Scholz, R., Buick, I.S., Gerdes, A., Kamo, S.L., Corfu, F., Marinho, M.M., Chaves, A.O., Valeriano, C., and Hermínio, A.N Jr., 2016, An assessment of monazite from the Itambé pegmatite district for use as U-Pb isotope reference material for microanalysis and implications for the origin of the "Moacyr" monazite: Chemical Geology, v. 424, p. 30-50.

Horstwood, M.S.A., Košler, J., Gehrels, G., Jackson, S.E., McLean, N.M., Paton, C., Pearson, N.J., Sircombe, K., Sylvester, P., Vermeesch, P., Bowring, J.F., Condon, D.J., and Schoene, B., 2016, Community-derived standards for LA-ICP-MS U-(Th-)Pb geochronology – uncertainty propagation, age interpretation and data reporting: Geostandards and geoanalytical research, v. 40, p. 311-332.

Knoper, M., Armstrong, R.A., Andreoli, M.A.G., and Ashwal, L.D., 2001, The Steekampskraal monazite vein: a subhorizontal stretching shear zone indicating extensional collapse of Namaqualand at 1033 Ma?: Journal of African Earth Sciences, v. 30.

Larson, K., 2021, ChrontouR: geochronology plotting scripts in R. https://osf.io/p46mb/. Last updated: 2021-10-05. DOI:10.17605/OSF.IO/P46MB

Lagos, M., Scherer, E.E., Tomaschek, F., Münker, C., Keiter, M., Berndt, M. J., and Ballhaus, C., 2007, High precision Lu-Hf geochronology of Eocene eclogite-facies rocks from Syros, Cyclades, Greece: Chemical Geology, v. 243, p. 16–35.

Münker, C., Weyer, S., Scherer, E.E., and Mezger, K., 2001, Separation of high field strength elements (Nb, Ta, Zr, Hf) and Lu from rock samples for MC-ICPMS measurements: Geochemistry, Geophysics, Geosystems, v. 2, 2001GC000183.

Paton, C., Hellstrom, J., Paul, B., Woodhead, J., and Hergt, J., 2011, Iolite: freeware for the visualisation and processing of mass spectrometric data: Journal of analytical atomic spectrometry, v. 26, p. 2508-2518.

Rubatto, D., 2017, Zircon: the metamorphic mineral: Reviews in Mineralogy and Geochemistry, v. 83, p. 261-295.

Scherer, E.E., Cameron, K.L., and Blichert-Toft, J., 2000, Lu-Hf garnet geochronology: Closure temperature relative to the Sm-Nd system and the effects of trace mineral inclusions: Geochemica et Cosmochimica Acta, v. 64, p. 3413–3432.

Scherer, E.E., Münker, C., and Mezger, K., 2001, Calibration of the Lutetium-Hafnium Clock: Science, v. 293, p. 683–687.

Sláma, J., Košler, J., Condon, D.J., Crowley, J.L., Gerdes, A., Hanchar, J.M., Horstwood, M.S.A., Morris, G.A., Nasdala, L., Norberg, N.,, Schaltegger, U., Schoene, B., Tubrett, M.N., and Whitehouse, M.J., 2008, Plešovice zircon—a new natural reference material for U-Pb and Hf isotopic microanalysis: Chemical Geology, v. 249, p. 1-35.

Söderlund, U., Patchett, P.J., Vervoort, J.D., and Isachsen, C.E., 2004, The ^{176}Lu decay constant determined by Lu–Hf and U–Pb isotope systematics of Precambrian mafic intrusions: Earth and Planetary Science Letters, v. 219, p. 311–324.

Sprung, P., Scherer, E.E., Upadhyay, D., Leya, I., and Mezger. K., 2010, Non-nucleosynthetic heterogeneity in non-radiogenic stable Hf isotopes: Implications for early solar system chronology: Earth and Planetary Science Letters, v. 295, p. 1–11.

Tomascak, P.B., Krogstad, E.J. and Walker, R.J., 1996, U-Pb monazite geochronology of granitic rocks from Maine: implications for late Paleozoic tectonics in the northern Appalachians: The Journal of Geology, v. 104, p. 185-195.

Vermeesch, P., 2018, IsoplotR: A free and open toolbox for geochronology: Geoscience Frontiers, v. 9, p. 1479-1493.

Vervoort, J.D., and Blichert-Toft, J., 1999, Evolution of the depleted mantle: Hf isotope evidence from juvenile rocks through time: Geochim Cosmochim Acta, v. 63(3–4), p. 533–556

Wiedenbeck, M., Allé, P., Corfu, F., Griffin, C.W.L., Meier, G.M., Oberli, F., von Quadt, A., Roddick, J.C., and Spiegel, W., 1995, Three natural zircon standards for U-Th-Pb, Lu-Hf, trace element and REE analyses: Geostandards Newsletter, v. 19, p. 1-23.